Available online at www.sciencedirect.com
SCIENCE DIRECT
Planetary and Space Science 54 (2006) 871–878
Planetary and Space Science
www.elsevier.com/locate/pss

Search for the putative dust belts of Mars: The late 2007 opportunity

Alexander V. Krivov*, Artem G. Feofilov, Valeri V. Dikarev

Astrophysical Institute and University Observatory, Friedrich Schiller University, Schillergaesschen 2–3, 07745 Jena, Germany

Received 25 October 2005; accepted 4 May 2006
Available online 5 July 2006

Abstract

The putative dust belts of Mars, a thin equatorial Phobos ring and a thick tilted Deimos torus, whose existence was predicted several decades ago, remain undiscovered. The previous attempt of direct observational detection, undertaken with the Hubble Space Telescope (HST) during the Mars equatorial plane crossing in May 2001, set an upper limit on the normal optical depth to $\sim 3 \times 10^{-8}$ for the Phobos ring and $\sim 10^{-7}$ for the Deimos torus. This paper analyzes possible reasons for non-detection of the belts and focuses on the next, and the last for three decades to come, natural opportunity to search for the dust belts during the Mars ring plane crossing in December 2007. We have extended our dynamical models to predict the appearance of both dust belts and to estimate the distribution of their optical depth and brightness. Our new calculations show that at least the Deimos dust torus may have escaped HST detection in 2001 only marginally. A thoroughly prepared observational attempt in 2007 with HST, Keck or another comparable telescope will have good chances to discover the Deimos torus, if a detector has a sensitivity by about one order of magnitude better than the one used in 2001. Photometric detection of the Phobos ring appears to be more difficult.

PACS: 96.30.Gc; 96.30.Wr

Keywords: Mars; Phobos; Deimos; Rings; Ejecta; Dynamics; Observations

1. Introduction

Soter (1971) first suggested that two tiny martian moons, Phobos and Deimos, should act as sources of dust for the circummartian space. The proposed mechanism of dust ejection from the satellite surfaces is their continuous hypervelocity bombardment by interplanetary micrometeoroids. Soter has shown that, owing to low escape speeds from the surfaces and high ejecta yields, a copious amount of dust should get injected in aerocentric orbits, forming tenuous tori around the orbits of the moons. In course of the subsequent theoretical studies by many authors, substantial improvements have been made to the models of the martian tori (see, e.g. Krivov and Hamilton, 1997, and references therein).

So far, only two dedicated photometric attempts have been undertaken to discover the dust belts observationally. The first one was made by the Viking Orbiter 1 spacecraft in 1980 (Duxbury and Ocampo, 1988) and brought a negative result, setting the upper limit of the normal optical depth of the putative tori to $\tau \lesssim 3 \times 10^{-5}$. The second one was made in May 2001, when the Hubble Space Telescope (HST) was used to search for the martian belts and unknown moonlets of Mars (Showalter et al., 2006). This attempt, also unsuccessful, reduced the upper limit to the normal optical depth to $\tau_\perp \lesssim 3 \times 10^{-8}$ for the Phobos torus and, more tentatively, $\tau_\perp \lesssim \times 10^{-7}$ for the Deimos torus (Showalter et al., 2006). Strictly speaking, constraints were put rather on the edge-on brightness of the hypothesized tori which, assuming geometric albedo of 0.07, translate to the limits on the edge-on optical depth: $\tau_\parallel \lesssim 2 \times 10^{-6}$ (Phobos) and $\tau_\parallel \lesssim 10^{-6}$ (Deimos). Assuming a certain geometry of the dust belts, these values were then converted to the limits on the normal optical depth $\tau_\perp$ quoted above. On any account, the new observational limits are already close to the upper limit suggested by the theory (Krivov and Hamilton, 1997).

*Corresponding author. Tel.: +49 3641 947530; fax: +49 3641 947512.
E-mail address: krivov@astro.uni-jena.de (A.V. Krivov).

0032-0633/$ - see front matter © 2006 Elsevier Ltd. All rights reserved.
doi:10.1016/j.pss.2006.05.007

There is some indication for the presence of dust from in situ measurements by the Phobos-2 spacecraft in the 1980s. During a Phobos orbit crossing, the magnetometer of Phobos-2 registered short-lasting fluctuations of the magnetic field and plasma parameters, called "Phobos events" (Dubinin et al., 1990). The Phobos events may indirectly evidence the presence of a dust torus around the Phobos orbit, although can be alternatively attributed to the presence of a gaseous rather than dusty torus (Dubinin, 1993; Baumgärtel et al., 1996). Magnetic field fluctuations were registered just before and right after the crossing of the Sun–Deimos line by the Phobos spacecraft as well ("Deimos event"). The Deimos event possibly indicates the existence of a dust or macromolecular cloud around Deimos itself (Sauer et al., 1995). Such a cloud acts as an obstacle to the solar wind and produces the Mach cone (a "plasma wake" in the solar wind downstream direction), during the crossing of which by the spacecraft the Deimos event was observed. However, these scarce facts cannot substitute direct in situ or remote sensing of the predicted dust belts.

In this paper, we focus on the observability of the putative martian dust belts from Earth during Mars plane crossings at opposition. We argue that at least the Deimos dust torus may have escaped HST detection in May 2001 only marginally. Given the observational conditions during the forthcoming Mars equatorial plane crossing at Mars opposition in the end of 2007 which are only slightly worse than in May 2001, and rapid improvement of detectors, another attempt with Keck or HST in 2007 would have good chances for success.

In Section 2, we outline essential properties of the martian dust belts, as expected from previous models. Our new model is described in Section 3. The updated model is used in Section 4 to estimate the expected mean optical depth of the dust belts and in Section 5 to calculate the distribution of optical depth and brightness of the dust belts during the upcoming Mars ring plane crossing in December 2007. Conclusions are made in Section 6.

2. Earlier predictions

Previous studies have shown that the dynamics, sinks, and lifetimes of dust debris lost by the martian moons strongly depend on the grain sizes. Accordingly, the whole dust complex formed by the Phobos and Deimos ejecta has been classified into four populations with distinctively different properties (Krivov, 1994; Krivov and Hamilton, 1997). Population 0 consists of the largest grains with radii $\gtrsim 1$ mm. Since these are subject to gravitational perturbations only, they stay within confined tori along the moons' orbits, the size of which is determined by the initial ejection velocity distribution (Kholshevnikov et al., 1993). As these particles rapidly re-accrete on the parent moon, their lifetimes and related number densities are very low. Population I contains smaller particles with radii from hundreds down to tens of microns. The dynamics in this size regime arise from the interplay between two perturbations, solar radiation pressure and planetary oblateness, resulting in extended asymmetric tori. The main loss mechanism of these grains is their occasional impacts with Phobos (for Phobos grains) and both martian moons (for Deimos ones), see Makuch et al. (2005). The lifetimes vary from tens of years (Phobos ejecta) to tens of thousands of years (Deimos debris). Below a certain critical radius, roughly ten microns, the particles collide with Mars at the pericenter of their orbits in less than 1 year, so they are present with low number densities. These grains are classified as Population II. Tiniest, submicron-sized fragments (Population III) are strongly influenced by electromagnetic forces and solar wind, are swept out from the vicinity of Mars in 10–100 days and form an extended, highly variable halo enveloping the martian system (Horányi et al., 1991). The properties of all four populations are summarized in Table 1.

As seen from the Table, the number densities, and therefore possible impact rates onto a dust detector aboard spacecraft near Mars, would be determined by Population II Phobos grains, Population I Deimos grains, as well as submicron particles of Population III from both satellites. For remote sensing, the picture is simpler. The cross section

Table 1
Populations of circummartian dust (Krivov, 1994; Krivov and Hamilton, 1997)

Pop.	Radii (μm)[a]	Perturbing forces[b]	Sinks	Lifetimes (years)	Shape	Number density[c]
0	$\gtrsim 1000$	J2	Parent moon	~ 1	Narrow tori	Low
I	10–1000 (P)	RP + J2	Parent moon	$\sim 10^2$ (P)	Equat. ring (P)	Med (P)
I	5–1000 (D)	RP + J2	Parent moon	$\sim 10^4$ (D)	Tilted torus (D)	High (D)
II	0.3–10 (P)	RP + J2	Mars	$\lesssim 1$	Asymm. ring	High (P)
II	0.3–5 (D)	RP + J2	Mars	$\lesssim 1$	Asymm. ring	Low (D)
III	$\lesssim 0.3$	EM + RP	IP space	~ 0.1?	Extended halo	High?

[a]For the dielectric material used in Makuch et al. (2005). The bulk density is 2.37 g cm^{-3}, the radiation pressure efficiency factor $Q_{pr} \approx 0.4$ for ~ 10 μm grains.

[b]J2 = Mars' oblateness, RP = radiation pressure, EM = electromagnetic (Lorentz) force.

[c]High: 10^4–10^5 km^{-3}, medium: $\sim 10^3$ km^{-3}, low: $\lesssim 10^2$ km^{-3}.

area, and therefore the optical depth and radiation fluxes, should be dominated by Population I grains.

In what follows, we confine our analysis to this Population I. Following Krivov and Hamilton (1997), we now summarize typical features that both dust belts are expected to have:

1. Both Deimos and Phobos belts change from one martian season to another, with the dependence being more pronounced for the Deimos belt. The Deimos torus is displaced away from the Sun, whereas the Phobos torus is shifted toward the Sun. The smaller the grains, the larger the displacements.
2. The Phobos dust belt is very thin and is more accurately called a ring than a torus. The sizes and shapes of the "partial" rings formed by different-sized Phobos ejecta exhibit a weak dependence on the grain radii. The Deimos torus, in contrast, is highly extended in the vertical direction. Smaller grains form thicker tori.
3. The Phobos ring is confined to the martian equatorial plane, but the plane of symmetry of the Deimos torus is tilted relative to the equator. This plane is always seen edge-on in the YZ-projection.
4. The distribution of dust in both dust belts—radial, azimuthal, and vertical—is very non-uniform.

As explained above, all these properties are explained by the interplay between the solar radiation pressure and planetary oblateness forces.

3. Updates to the model of the dust belts

To study the observability of the martian dust belts in this paper, we employed our dynamical code that numerically integrates orbit-averaged equations of motion of a circummartian particle in Lagrange elements derived by Krivov et al. (1996) and used by Krivov and Hamilton (1997), which we recently generalized to accommodate the Poynting–Robertson drag (Makuch et al., 2005). In addition, we included here another effect—the modulation of the radiation pressure force by the orbital eccentricity of Mars, $e_{\mathrm{M}} = 0.093$—an effect, whose existence was first pointed out by Juhász and Horányi (1995) then discussed by Krivov et al. (1996), Hamilton (1996) and, most recently, re-addressed by Showalter et al. (2006). The final version of the equations of motion with both the Poynting–Robertson drag and e_{M} included, is given in the Appendix. These equations were carefully tested against direct integrations of equation of motion in coordinates, showing a perfect agreement. The usage of the orbit-averaged equations reduces the integration time by a factor of 10–100, enabling us to construct composite models based on merging the results for many particles launched with different initial data.

These equations of motion were integrated simultaneously with a differential equation that describes probability of particle's loss due to collisions with the martian moons. The launch times of particles were uniformly distributed between the observation epoch and a sufficiently distant limit in the past, chosen so that the particles ejected then do not survive until the present time. For Phobos, the distant limit was set to 100 m.y. (martian years). For Deimos, the limit of 100,000 m.y. was necessary. In the present epoch, the final orbits together with the dust production rate N^{+} and probabilities of particle's loss to collisions with moons were used to construct 3D arrays that contain the present-day number densities of dust particles around Mars.

As far as the influence of Mars' eccentricity is concerned, our results are in agreement with those of Showalter et al. (2006) after accounting for the difference in the adopted density and radiation pressure efficiency of dust grains. Inclusion of e_{M} has little effect on the Deimos ejecta, slightly increasing the critical radius from 5 to about 7 μm. However, it does have tangible and diverse consequences for the Phobos grains. Depending on the solar longitude at the moment of ejection, the time to collision with Mars can be greatly extended or reduced with respect to that of a hypothetical particle moving about the planet on a circular orbit around the Sun. A minor fraction of Phobos grains of radii down to 8 μm can orbit Mars without striking it for more than 100 m.y. and conversely, some of the 50 μm-sized particles are still driven to collision with the planet in less than 100 m.y. Typically, the lifetimes against collision with Mars are longer than the lifetimes against collisions with moons (~20 m.y. for Phobos) for 20 μm-sized and bigger ejecta.

Smaller particles are produced at much higher rates than larger ones, and the lifetimes of grains against impacts to the martian moons decrease with the increasing size. Therefore, the cross section area in the belts will be dominated by particles somewhat larger than the critical radii (Makuch et al., 2005). In the subsequent estimates of the production rates we take reasonably narrow size ranges above the critical sizes, $[20, 30]$ μm for Phobos and $[10, 15]$ μm for Deimos. In the numerical integrations, we use one size: 20 μm for Phobos and 10 μm for Deimos.

Fig. 1 depicts the dust belts of both martian moons at the moment of the martian spring equinox. Shown is the projection onto the equatorial plane, with Sun to the right. This simulation, as all others in this paper, reproduces only the partial "belts" made up by particles with radii just above the critical value: 20 μm for Phobos and 10 μm for Deimos. As expected, the Deimos torus is displaced in the anti-solar direction. However, the Phobos ring is no longer displaced in the solar direction. Taking the Mars eccentricity into account leads to its symmetrization. This is explained by the fact that, with $e_{\mathrm{M}} \neq 0$, the orbital eccentricity of the Phobos grains no longer experiences oscillations with periodic returns to zero. Instead, after some period of evolution the eccentricity typically starts to oscillate at relatively high values, up to 0.6 for 20 μm particles, and the apsidal line of an elliptic orbit starts to circulate instead of librating, as was the case with $e_{\mathrm{M}} = 0$.

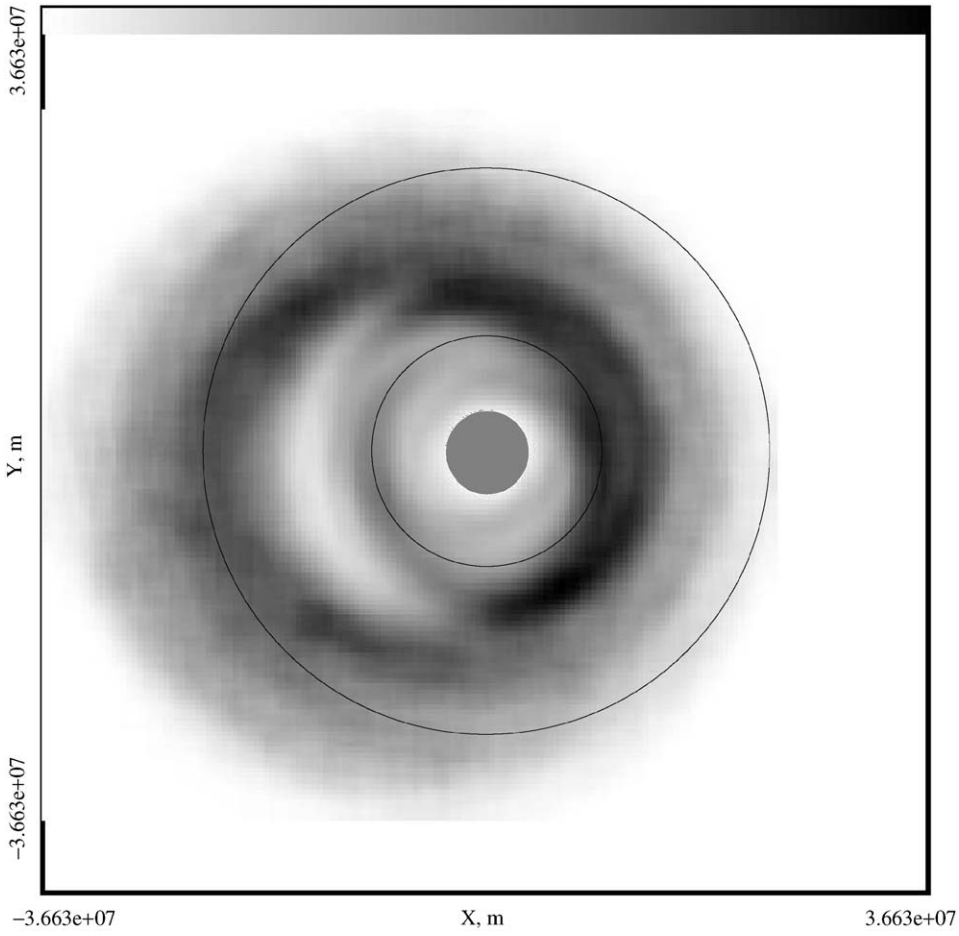

Fig. 1. Both dust belts in martian spring, projected onto the equatorial plane of Mars. Circles mark Mars itself and the orbits of Phobos and Deimos. X-axis points toward Mars' vernal equinox point (coincides with the direction toward the Sun). We used scatter plots produced by numerical integration routine for 20 μm-sized Phobos and 10 μm-sized Deimos grains, distributed 250,000 instantaneous positions of particles into 135×135 bins in the XY-plane, and used sliding averaging over three adjacent bins in each direction. For each of the two belts greyscale is proportional to the column density of dust particles. However, the column density of the Phobos dust is artificially increased by a factor of 50 (otherwise the Phobos torus would not be visible in the plot).

In terms of phase portraits "eccentricity–solar angle" discussed by Hamilton and Krivov (1996), the grain starts to follow one of the outer circles shown in their Fig. 7f.

For the sizes just above the critical radii, the pericenters of the particle orbits are close to the martian surface. Therefore, the belts nearly touch the surface: the Phobos ring at all azimuthal angles, the Deimos torus at the subsolar point. Both belts significantly overlap in space. As in previous simulations, the Deimos torus is tilted to the equatorial plane, which is not seen in the figure. For a full set of snapshots, in three projections and for four martian seasons, see Figs. 1 and 3 in Krivov and Hamilton (1997).

4. Optical depth of the dust belts

To estimate how dense the dust belts could be, a quantity of primary interest is the dust production rate from the satellite surfaces. We use a procedure described, e.g., in Section 2 of Krivov et al. (2003). The mass flux and typical speeds of micrometeoroid impactors at Mars are taken to be (Grün et al., 1985; Divine, 1993)

$$F_{\rm imp} \approx 1 \times 10^{-16}\,{\rm g\,cm^{-2}\,s^{-1}} \quad \text{and} \quad v_{\rm imp} = 15\,{\rm km\,s^{-1}}. \quad (1)$$

For this impact speed, assuming 10^{-5} g as a typical mass of projectiles and a "silicate" surface, the plausible yield is (Koschny and Grün, 2001)

$$Y \approx (3-7) \times 10^2. \quad (2)$$

Denoting by S the cross section area of a satellite, we obtain the mass production rate from the moon surface:

$$M^+ = F_{\rm imp}\, YS, \quad (3)$$

or $0.14-0.32\,{\rm g\,s^{-1}}$ for Phobos and 0.05 —$0.11\,{\rm g\,s^{-1}}$ for Deimos.

Taking the size distribution to be a standard power law with the index -3.5 and the mass of the heaviest ejecta fragment to be $\sim 10^{-5}$ g, we finally find the production rate of [20, 30] μm-sized Phobos grains and [10, 15] μm-sized Deimos particles to have comparable values between $N^+ \sim 10^5$ and $\sim 10^6\,{\rm s^{-1}}$. (A larger S of Phobos, compared

to Deimos, nearly compensate for larger radii and therefore lower production rates of Phobos particles.) Due to low escape velocities from the surfaces of both moons ($<10\,\mathrm{m\,s^{-1}}$), a sizeable fraction of ejecta should escape. In what follows, we adopt

$$N^{+}\sim 10^{5}\,\mathrm{s^{-1}}, \tag{4}$$

which is a "cautious" or "reasonably pessimistic" estimate. Still, one should keep in mind that the parameter N^{+} is very uncertain.

Combining the dust production rate with knowledge of dynamics (typical eccentricities and inclinations of the particles, lifetimes against collisions with the moons etc.), one can easily estimate the optical depth of the belts (see Section 3.2 of Krivov and Hamilton, 1997 and Section 4.2 of Makuch et al., 2005 for explicit formulas). The results, presented in Fig. 2 (dashed lines), are consistent with the recent non-detection of the tori (Showalter et al., 2006). In the "cautious" case ($N^{+}\sim 10^{5}\,\mathrm{s^{-1}}$) the optical depth of the Phobos ring (Deimos belt) is by two (one) order(s) of magnitude below the observational limits of 2001.

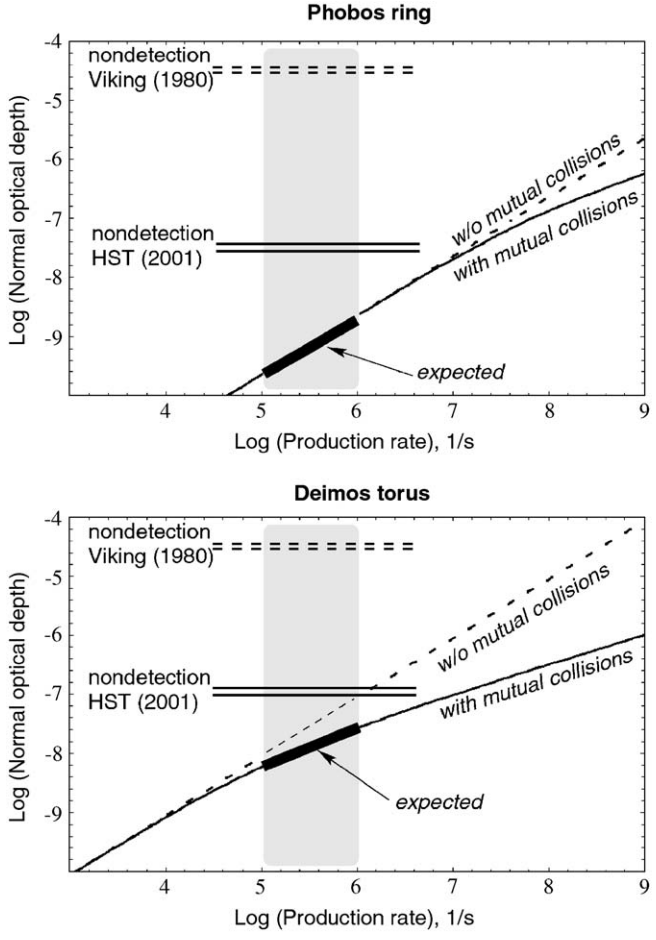

Fig. 2. Expected normal optical depth of the Phobos (top) and Deimos (bottom) dust tori, as a function of the (vaguely known) production rate of particles that make the largest contribution to the optical depth (radii from 20 to 30 μm for Phobos and from 10 to 15 μm for Deimos). The plausible range of this production rate is hatched. Dashed and solid lines: models without and with mutual collisions of the torus particles. Horizontal double dashed and double solid lines mark upper limits of the optical depth set by observations with Viking cameras in 1980 (Duxbury and Ocampo, 1988) and Hubble Space Telescope in 2001 (Showalter et al., 2006).

We now obtain more accurate estimates of the optical depths, by taking into account effects of mutual collisions of the torus particles which, as Makuch et al. (2005) showed, may be important for the Deimos torus. The results are depicted in Fig. 2 with solid lines. Comparison with dashed lines, computed without taking collisions into account, shows that collisions may indeed reduce the optical depth of the Deimos torus (bottom panel) by a factor of several for a higher production rate $N^{+}\sim 10^{6}\,\mathrm{s^{-1}}$. For the "cautious" value of $10^{5}\,\mathrm{s^{-1}}$, however, the difference is less than a factor of two. Besides, the collisions weaken the dependence of the optical depth on N^{+}. This helps making predictions: the uncertainty of the optical depth turns out to be less than the uncertainty in the production rate. The fact that collisional lifetimes of Deimos grains are comparable to their lifetimes against accretion by satellites may reinforce discussion of possible self-sustainment of the Deimos torus—an idea proposed by Sasaki (1994) more than 10 years ago. In contrast, mutual collisions of grains in the Phobos torus (top panel in the same figure) are unimportant.

5. Observability of the dust belts: discovery in late 2007?

The Phobos ring lies in the equatorial plane of Mars. The symmetry plane of the Deimos torus is tilted to the equator, but its line of nodes coincides with the direction to the Mars' vernal equinox (Hamilton, 1996; Krivov and Hamilton, 1997). This implies that both belts are seen edge-on, and have the maximum optical depth, during Mars' equatorial plane crossings. Of course, the chances to detect the belts are the best if a plane crossing occurs close to opposition, when geocentric distance to the planet is at a minimum.

The previous event of plane crossing near opposition took place in May 2001 when the minimum geocentric distance was 0.5 AU. As Showalter et al. (2006) pointed out, the next one will occur in December 2007, though at a somewhat larger distance of 0.6 AU. Still, it offers the best chance to look for the martian dust belts observationally for many years to come: the next opportunity will not be until July 2033. Fig. 10 in Showalter et al. (2006) depicts the details of the viewing geometry during the upcoming plane crossing in late 2007. On December 19, 2007 the geocentric distance to Mars reaches a minimum of 0.589 AU. The minimum phase angle of about 2.1° is on December 25, 2007. The opening angle of the Mars' equatorial plane reaches zero on January 01, 2008 and then once again on February 29, 2008. The best time window for Phobos dust ring searches would be the week between Christmas 2007 and New Year Day 2008. For the Deimos torus the window may be broader, extending to a few

weeks in December 2007–January 2008. See Showalter et al. (2006) for further details.

Fig. 3 shows the distribution of geometrical optical depth of the Phobos ring (top) and Deimos torus (bottom), as seen from Earth in December 2007. It is striking how dissimilar both dust complexes are: the Phobos complex is indeed a thin equatorial ring with sharp edges, whereas the Deimos belt is a tilted torus with larger radial and *much* larger vertical extent and fuzzy boundaries. Four "blobs" seen in the Deimos torus "image" have the same origin as the classical IRAS dust bands (e.g., Dermott et al., 2001). They reflect the fact that the dust grains spend much time at the extremes of their vertical excursions. Since these extremes are controlled by the inclination, which itself varies sinusoidally, the blobs are somewhat blurred.

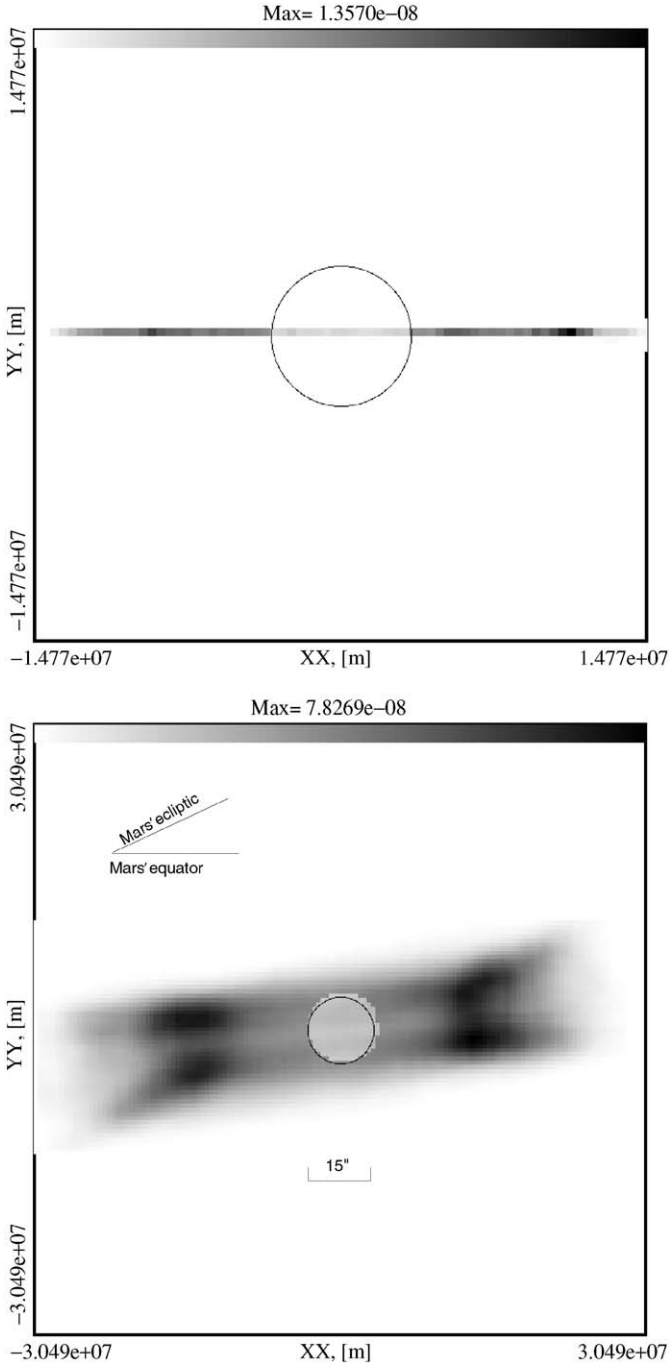

Fig. 3. Distribution of the optical depth of (or radiation fluxes from) the Phobos ring (top) and Deimos torus (bottom), as seen during the observations from Earth in December 2007. Pixel size adopted: $1'' \times 1''$. Note different scales on the two panels: each is adjusted to the spatial extent of the corresponding dust belt.

We have also calculated the fluxes of scattered radiation in the visual and near-infrared (thermal emission at these wavelengths is negligible). The particles under study, tens of micrometers in size, all have the size parameters $\gg 1$ and are strong forward-scatterers. In that sense, the Earth-borne observations at Mars opposition are not advantageous, but there is no other option: observations in forward scatter are only possible for interior planets, namely at inferior conjunctions. Since the phase angles for all parts of the tori are nearly the same, very close to 0° (backscatter), the resulting 2D distributions look almost identical to those of the optical depth (Fig. 3) and are not shown here.

We now return to the most uncertain part of the modeling: expected absolute values of the geometrical optical depth and the radiation fluxes. To the uncertainties that come from the conjectured dust production rate from the satellite surfaces, those coming from vaguely known optical properties of particles have to be added. Below we report estimates obtained with "reasonably pessimistic" assumptions about the dust production, with the caveat that they are uncertain by at least one order of magnitude, perhaps even more.

The mean (i.e., spatially averaged) geometrical optical depth is of the order of 2×10^{-8} for the Deimos torus and 2×10^{-9} for the Phobos ring. The total fluxes within the spectral window from $\lambda = 0.5$ to $2.0\,\mu$m, integrated over each belt, are much more different: $\sim 3 \times 10^{-10}\,\mathrm{erg\,cm^{-2}\,s^{-1}}$ for Deimos and $\sim 1 \times 10^{-12}\,\mathrm{erg\,cm^{-2}\,s^{-1}}$ for Phobos. The specific flux from the Deimos torus, integrated over the whole belt, is about 40 mJy at both 0.5 and $2.0\,\mu$m and reach a maximum of about 60 mJy at the wavelength of $\approx 1\,\mu$m. The latter is explained by the fact that the radiation expected from the dust belts is essentially the scattered solar radiation, whose flux in Jansky (i.e., in the frequency scale) peaks at that wavelength. For the Phobos ring, the flux varies from about 0.1 mJy at both 0.5 and $2.0\,\mu$m to about 0.2 mJy at $1\,\mu$m.

The main reason for the much higher spatially integrated fluxes for the Deimos torus is the much longer lifetimes of Deimos' particles compared to Phobos' ones, so that the Deimos belt contains much more material than the Phobos belt. However, the Deimos dust is distributed over a much larger volume in space than the Phobos ejecta and accordingly, the Deimos torus occupies a much larger area on the celestial sphere than the Phobos ring. As a consequence, the maximum optical depth (up to $\sim 10^{-7}$ for the Deimos torus and up to $\sim 2 \times 10^{-8}$ for the Phobos ring) and the maximum flux per pixel (up to $\sim 2 \times 10^{-13}\,\mathrm{erg\,cm^{-2}\,s^{-1}\,arcsec^{-2}}$ for the Deimos torus and up to $\sim 3 \times 10^{-14}\,\mathrm{erg\,cm^{-2}\,s^{-1}\,arcsec^{-2}}$ for the Phobos ring)

differ only by a factor of several. It should be emphasized that this conclusion is only valid very close to the ring plane crossing. Far from it, the optical depth and flux per pixel for the Phobos ring may be by two orders of magnitude lower than those for the Deimos torus, ruling out any chance to detect the Phobos ring.

6. Conclusions

The putative dust belts of Mars whose existence was predicted several decades ago are still waiting for direct observational detection. The last attempt, undertaken with HST during the Mars equatorial plane crossing in May 2001, set an upper limit on the normal optical depth to $\sim 3 \times 10^{-8}$ for the Phobos ring and $\sim 10^{-7}$ for the Deimos torus. This corresponds to limits of the edge-on-optical depth of 2×10^{-6} (Phobos) and 10^{-6} (Deimos). The primary goal of this paper was to find out, how good are chances for success during the forthcoming plane crossing at Mars opposition in the end of 2007. Our main findings are as follows:

1. In December 2007, the Deimos torus would occupy on the celestial sphere a nearly rectangular, slightly wedged area symmetric about Mars, with fuzzy boundaries. Its vertical extent is $\sim 4R_{\mathrm{M}} \sim 30''$ ($R_{\mathrm{M}} = 7.9'' =$ angular radius of Mars in December 2007) and a radial extent is $\sim 14R_M \sim 110''$. The symmetry plane of the torus image would be tilted by some 10° to the equatorial plane toward the ecliptic and therefore should lie between the equatorial and ecliptic planes. The image should be dominated by four bright "blobs" about $4-5R_{\mathrm{M}}$ $\sim 30-40''$ away from Mars on both sides of it. If the angular resolution is less than a few arcseconds, only two bright spots can be seen—one on each side of Mars. In contrast, the Phobos ring would appear as a thin ($\sim 1''$) segment confined to the equatorial plane and lying fully inside the Deimos torus.
2. The optical depth and surface brightness (per pixel) of the Deimos torus at the plane crossing should be by only a factor of several larger than those of the Phobos ring. However, the spatially integrated flux from the Deimos torus must be by two orders of magnitude larger. As a result, the thin Phobos ring could be hardly visible on the Deimos torus background, especially if the angular resolution of instrument is low ($\gtrsim 1''$), or if the opening angle at the observation moment slightly differs from zero.
3. The absolute values of the optical depth and brightness of both belts are very uncertain. The "reasonably pessimistic" estimates give the mean geometric optical depth of both tori of about 2×10^{-8} for the Deimos torus and 2×10^{-9} for the Phobos ring (cf. the 2001 upper limits of edge-on optical depth). The optical depth in the "blobs" of the Deimos torus may be $\approx 1 \times 10^{-7}$. The spatially integrated specific fluxes from the Deimos torus in the visual and near-infrared may be of the order of 40–60 mJy, from the Phobos ring about 0.1–0.2 mJy. The peak fluxes per pixel, integrated over the spectral window 0.5–2.0 μm, are estimated as $\sim 2 \times 10^{-13}\,\mathrm{erg\,cm^{-2}\,s^{-1}\,arcsec^{-2}}$ for the Deimos torus and $\sim 3 \times 10^{-14}\,\mathrm{erg\,cm^{-2}\,s^{-1}\,arcsec^{-2}}$ for the Phobos ring. Optimistic estimates of all the quantities listed could be by about one order of magnitude higher.

Given these results, another observational attempt with HST, Keck or comparable instruments would have good chances to discover at least the Deimos torus. A condition for that is a detector with a sensitivity by about one order of magnitude better than the one used in 2001. One can further increase chances for success by choosing the optimal signal-to-noise ratio per pixel versus the desired resolution. This is especially important for the Deimos torus to avoid "overresolving" it (Imke de Pater, personal communication).

Acknowledgments

We appreciate useful discussions with Mark Showalter and Imke de Pater, who also provided helpful reviews of this manuscript. This research was supported by Deutsche Forschungsgemeinschaft (DFG), project Kr 2164/1-3. The paper was presented at the Workshop "Physics of Dusty Rings" (Bern, Switzerland, June 20–24, 2005), funded by the International Space Science Institute (ISSI).

Appendix A. Orbit-averaged equations of motion

Considering the motion of a particle around a planet under the action of two perturbing forces, solar radiation pressure and planetary oblateness, Krivov et al. (1996) derived orbit-averaged equations of motion in Lagrange elements h, k, p, q, defined as

$$h = e\cos\tilde{\omega}, \quad k = e\sin\tilde{\omega}, \quad p = \sin i\cos\Omega, \quad q = \sin i\sin\Omega, \tag{A.1}$$

where $\tilde{\omega} = \Omega + g$ is the longitude of pericenter and e, i, Ω, g are eccentricity, inclination, longitude of the ascending node, and argument of pericenter, respectively. To make the equations of motion dimensionless, they used the mean longitude of the Sun $\lambda_{\odot}$ instead of time as an independent variable. This quantity $\lambda_{\odot}$ is a linear function of time:

$$\lambda_{\odot} = \lambda_{\odot 0} + n_{\odot} t, \tag{A.2}$$

where $\lambda_{\odot 0}$ is the initial solar longitude at the moment of ejection ($t = 0$). Later on, Makuch et al. (2005) added the equation for semimajor axis a to accommodate the Poynting–Robertson drag. We now further generalize the equations to include the orbital eccentricity of the planet. The generalization is rather straightforward, and the result reads:

$$\frac{\mathrm{d}a}{\mathrm{d}\lambda_{\odot}} = -Da, \tag{A.3}$$

$$\frac{dh}{d\lambda_\odot} = -k\omega\frac{5I^2-2I-1}{2E^4} - \frac{C}{E(1+I)}\{[p-Hh]q\cos l_\odot + [E^2(1+I)-p(p-Hh)]\cos\varepsilon\sin l_\odot + [E^2(1+I)p-IKk]\sin\varepsilon\sin l_\odot\}, \quad (A.4)$$

$$\frac{dk}{d\lambda_\odot} = h\omega\frac{5I^2-2I-1}{2E^4} + \frac{C}{E(1+I)}\{[q-Hk]p\cos\varepsilon\sin l_\odot + [E^2(1+I)-q(q-Hk)]\cos l_\odot - [E^2(1+I)q-IKh]\sin\varepsilon\sin l_\odot\}, \quad (A.5)$$

$$\frac{dp}{d\lambda_\odot} = q\omega\frac{I}{E^4} + \frac{C}{E(1+I)}[Hp-(1+I)h] \times [(p\cos\varepsilon - I\sin\varepsilon)\sin l_\odot - q\cos l_\odot], \quad (A.6)$$

$$\frac{dq}{d\lambda_\odot} = -p\omega\frac{I}{E^4} + \frac{C}{E(1+I)}[Hq-(1+I)k] \times [(p\cos\varepsilon - I\sin\varepsilon)\sin l_\odot - q\cos l_\odot]. \quad (A.7)$$

Here, C, ω, and D are force parameters discussed below, ε denotes the obliquity of the planet, and we have denoted for brevity

$$E=\sqrt{1-e^2}=\sqrt{1-h^2-k^2}, \quad I=\cos i=\sqrt{1-p^2-q^2},$$

$$H=hp+kq, \quad K=hq-kp. \quad (A.8)$$

Another quantity that appears in the equations, $l_\odot$, is the *true* longitude of the Sun, computed from the mean longitude $\lambda_\odot$ by solving Kepler's equation with the orbital eccentricity of the planet as a parameter. The true longitude replaces the mean longitude in the previous versions of the equations (Krivov et al., 1996; Makuch et al., 2005).

The quantities C and ω are dimensionless parameters that characterize the strength of the radiation pressure and oblateness, respectively (see Krivov et al., 1996, for an exact definition) whereas D describes the Poynting–Robertson drag (see Makuch et al., 2005 for an explicit formula). The first two parameters, C and ω, are functions of semimajor axis a. The parameter D, in addition, has a weak dependence on the inclination i. Besides, C and D are proportional to the solar radiation flux, which is inversely proportional to the square of planet's heliocentric distance, which was treated as constant in the equations of Krivov et al. (1996) and Makuch et al. (2005). Here, we calculate it as a function of $\lambda_\odot$. Explicit dependence of these two parameters on $\lambda_\odot$ is another difference between our current equations and the previous ones.

References

Baumgärtel, K., Sauer, K., Bogdanov, A., Dubinin, E., Dougherty, M., 1996. Phobos events signatures of solar wind dust interaction. Planet Space Sci. 44, 589–601.

Dermott, S.F., Grogan, K., Durda, D.D., Jayaraman, S., Kehoe, T.J.J., Kortenkamp, S.J., Wyatt, M.C., 2001. Orbital evolution of interplanetary dust. In: Grün, E., Gustafson, B.Å.S., Dermott, S., Fechtig, H. (Eds.), Interplanetary Dust. Springer, Berlin, pp. 569–639.

Divine, N., 1993. Five populations of interplanetary meteoroids. J. Geophys. Res. 98, 17029–17048.

Dubinin, E.M., 1993. The Phobos and Deimos effects. Adv. Space Res. 13 (10), 271–290.

Dubinin, E.M., Lundin, R., Pissarenko, N.F., Barabash, S.V., Zakharov, A.V., Koskinen, H., Schwingenshuh, K., Yeroshenko, Y.G., 1990. Indirect evidences for a gas/dust torus along the Phobos orbit. Geophys. Res. Lett. 17, 861–864.

Duxbury, T.C., Ocampo, A.C., 1988. Mars: satellite and ring search from Viking. Icarus 76, 160–162.

Grün, E., Zook, H.A., Fechtig, H., Giese, R.H., 1985. Collisional balance of the meteoritic complex. Icarus 62, 244–272.

Hamilton, D.P., 1996. The asymmetric time-variable rings of Mars. Icarus 119, 153–172.

Hamilton, D.P., Krivov, A.V., 1996. Circumplanetary dust dynamics: effects of solar gravity, radiation pressure, planetary oblateness, and electromagnetism. Icarus 123, 503–523.

Horányi, M., Tátrallyay, M., Juhász, A., Luhmann, J.G., 1991. The dynamics of submicron-sized dust particles lost from Phobos. J. Geophys. Res. 96, 11283–11290.

Juhász, A., Horányi, M., 1995. Dust torus around Mars. J. Geophys. Res. 100, 3277–3284.

Kholshevnikov, K., Krivov, A.V., Sokolov, L.L., Titov, V.B., 1993. The dust torus around Phobos orbit. Icarus 105, 351–362.

Koschny, D., Grün, E., 2001. Impacts into ice-silicate mixtures: crater morphologies volumes depth-to-diameter ratios and yield. Icarus 154, 391–401.

Krivov, A.V., 1994. On the dust belts of Mars. Astron. Astrophys. 291, 657–663.

Krivov, A.V., Hamilton, D.P., 1997. Martian dust belts: waiting for discovery. Icarus 128, 335–353.

Krivov, A.V., Sokolov, L.L., Dikarev, V.V., 1996. Dynamics of Mars-orbiting dust: effects of light pressure and planetary oblateness. Celest. Mech. Dyn. Astron. 63, 313–339.

Krivov, A.V., Sremčević, M., Spahn, F., Dikarev, V.V., Kholshevnikov, K.V., 2003. Impact-generated dust clouds around planetary satellites: spherically symmetric case. Planet. Space Sci. 51, 251–269.

Makuch, M., Krivov, A.V., Spahn, F., 2005. Long-term dynamical evolution of dusty ejecta from Deimos. Planet Space Sci. 53, 357–369.

Sasaki, S., 1994. Martian dust tori formation: ejecta at collision of torus particles with the satellite can sustain the dust abundance. in: Shimitzu, M. and Mizutani, M. (Eds.), Proceedings of the 27th ISAS Lunar and Planetary Symposium, pp. 47–50.

Sauer, K., Dubinin, E., Baumgärtel, K., Bogdanov, A., 1995. Deimos: an obstacle to the solar wind. Science 269, 1075–1078.

Showalter, M.R., Hamilton, D.P., and Nicholson, P.D., 2006. A deep search for martian dust rings and inner moons using the Hubble Space Telescope. Planet. Space Sci., this issue.

Soter, S., 1971. The dust belts of Mars. Report of Center for Radiophysics and Space Research No. 462.